ISSN 1063-780X, Plasma Physics Reports, 2007, Vol. 33, No. 12, pp. 995–1013. © Pleiades Publishing, Ltd., 2007.
Original Russian Text © N.V. Baranets, Ya.P. Sobolev, M. Ciobanu, J. Vojta, J. Smilauer, Z. Klos, H. Rothkaehl, A. Kiraga, K. Kudela, J. Matišin, V.V. Afonin, B.S. Ryabov, N.V. Isaev, 2007, published in Fizika Plazmy, 2007, Vol. 33, No. 12, pp. 1086–1106.

BEAMS IN PLASMA

Development of Beam–Plasma Instability during the Injection a Low-Energy Electron Beam into the Ionospheric Plasma

N. V. Baranets[a], Ya. P. Sobolev[a], M. Ciobanu[b], J. Vojta[c], J. Smilauer[c], Z. Klos[d], H. Rothkaehl[d], A. Kiraga[d], K. Kudela[e], J. Matišin[e], V. V. Afonin[f], B. S. Ryabov[a], and N. V. Isaev[a]

[a] *Institute of Terrestrial Magnetism, Ionosphere, and Radio Wave Propagation, Russian Academy of Sciences, Troitsk, Moscow oblast, 142190 Russia*

[b] *Institute for Gravitation and Space Sciences, 71111 Bucharest, Romania*

[c] *Institute of Atmospheric Physics, Academy of Sciences of the Czech Republic, 14131 Prague 4, Czech Republic*

[d] *Space Research Center, Polish Academy of Sciences, 00-716 Warsaw, Poland*

[e] *Institute of Experimental Physics, Slovak Academy of Sciences, 04001 Košice, Slovakia*

[f] *Space Research Institute, Russian Academy of Sciences, Profsoyuznaya ul. 84/32, Moscow, 117997 Russia*

Received December 5, 2006; in final form, April 16, 2007

Abstract—Results are presented from an active experiment on the injection of charged particle beams into the ionospheric plasma. The experiment was carried out in 1992 onboard the *Intercosmos-25* satellite and the *Magion-3* daughter satellite (APEX). A specific feature of this experiment was that both the ion and electron beams were injected upward, in the same direction along the magnetic field. The most interesting results are the excitation of HF and VLF–LF waves and the generation of fast charged particle flows, which were recorded on both satellites.

PACS numbers: 52.35.Qz

DOI: 10.1134/S1063780X07120057

1. INTRODUCTION

In carrying out active experiments on the injection of charged particle beams from the *Interkosmos-25* (*IK-25*) automatic universal orbital station (AUOS), the main attention was paid to unmodulated electron injection from the UÉM electron gun (EG) and the simultaneous injection of a quasineutral xenon plasma jet and neutral xenon release from the UPM stationary plasma thruster (SPT) [1, 2]. The superposition of the effects induced in the ambient plasma during the joint operation of the injectors made the interpretation of these experiments rather difficult. However, in some experiments in which the injectors operated asynchronously, it was possible to separate spatiotemporal effects caused by the injection of the electron and ion beams. This was demonstrated by using the results of the experiment carried out at the 277th turn. A specific feature of this experiment was that charged particles were injected at pitch angles corresponding to the opposite propagation directions of the electron and ion beams along the magnetic field. Here, we consider another injection configuration in which the particle beams propagated in the same direction along the magnetic field; specifically, the particle beams simultaneously injected into the ionospheric plasma along the magnetic field $\mathbf{B}_0$ were nested in one another. The development of beam–plasma instability (BPI) under these conditions is of great interest, because electron beam injection through an ion beam results in the formation of a pronounced spatiotemporal structure. The mutual influence of the injected beams can have a significant effect on the development of instability if the frequencies of the excited waves are close to one another or these waves are parametrically coupled. The present study focuses on the high-frequency (HF) beam–plasma instability during electron beam injection.

Here, we also consider the effects observed in previous experiments [1] on the excitation of quasi-steady magnetic fields during electron injection, because these effects take place (though in a somewhat different form) under other experimental conditions as well. Some effects accompanying electron beam injection are most pronounced in the vicinity of the satellite, in the region with an enhanced ion-acoustic and Langmuir turbulence, which stimulates the focusing of the injected electron beam. The other effects are distributed over the entire interaction region and can be detected with higher probability by diagnostics installed on a subsatellite. Many parameters of electron injection in our experiment are close to those of the *Polar-5* rocket probe experiment carried out according to the parent–

Main parameters of the beam–plasma system in the ionosphere

Unperturbed plasma density, cm^{-3}	$n_0 \approx n_{ix}(V \le 1\ V)$	$(3–4) \times 10^3$
Electron temperature components in the unperturbed plasma, K	T_{ex}, T_{ey}, T_{ez}	2000, 1050, 1000
Electronic Debye length, cm	r_{De}	9–14
Injection currents of xenon ions and electrons, A	I_{bi}, I_{be}	2.1–2.4, 0.1
Maximum electron accelerating voltage, kV	U_0	10
EG power in 23-s injection cycles, %	$I_{be}U_0$	30, 60, 90
Alfvén velocity and flow velocities of electrons and xenon ions, m/s	u_A, u, u_{iz}	7.5×10^6, 4.2×10^7, 1.1×10^4
Average transverse dimensions of the ion and electron beams, m	r_{cx}, r_{ce}	280, 11
Thicknesses of the ion and electron hollow flows, m	δr_{cx}, δr_{ce}	150–210, 1.3–2.5
Estimated densities of the injected electrons (60% power) and xenon ions, cm^{-3}	n_{be}, n_{bi}	40–300, $(3–5) \times 10^3$
Gyrofrequency of xenon ions, Hz	ω_{cx}	14–20
Plasma frequency of the beam ions, Hz	ω_{px}	13–16
Gyrofrequency of the hydrogen plasma component, kHz	ω_{ci}	1.9–2.5
Plasma frequency of the hydrogen plasma component, MHz	ω_{pi}	0.09–0.11
Electron gyrofrequency, MHz	ω_{ce}	3.4–4.4
Electron plasma frequency of the unperturbed plasma, MHz	ω_{pe}	5.6–6.5
Plasma frequency of the beam electrons in the dc injection mode, MHz	ω_{be}	0.4–0.9
Modulation frequency of the electron current during 2–12 s of ac injection (after 1s of dc injection), Hz	$\omega_m/2\pi$	32–250000
Duration of the electron beam micropulse during ac injection, μs	τ_i	2

daughter scheme [3]. The first satellite experiments with low-power EGs were aimed at controlling the electric potential of the conducting satellite surface in order to reduce the influence of its negative charge on electric field measurements, studying the excitation of plasma waves in the ionosphere, and measuring longitudinal electric fields in the magnetosphere. The results from these experiments were presented in many original and review articles (see, e.g., [4, 5]).

2. SCIENTIFIC EQUIPMENT AND SPATIAL CONFIGURATION OF THE EXPERIMENT

Let us briefly describe the characteristic features of the scientific equipment used. The ion injector was a Hall SPT with a longitudinal acceleration of xenon ions. The injection current was 2.0–2.6 A, and the output ion energy was up to 250 eV. The ion injector differed from similar injectors used as propulsion engines only in a larger range of pitch angles. The electron injector was a straight-channel three-electrode EG operating at modulation frequencies varying from 32 Hz to 250 kHz (over a time period of 2–12 s) after the 1st second of dc injection, with 1-s intervals between the injection cycles. The EG control electrode provided 100% modulation of the electron beam current, thereby forming separate injection micropulses with a duration of 2 μs. The main characteristics of the injectors are given in the table. The components $E_{x,y,z}$ of the quasi-steady electric field (in the frequency ranges 0.1–2 and 0.1–10 Hz) and the very-low-frequency (VLF) alternating electric field $\mathbf{e}_{lf}$ (8 Hz–15.0 kHz) were measured by the DEP-2 apparatus and the NVK-ONCh wave complex, respectively, by using a system of double electric probes, the signals from which were fed to both devices. For example, the component E_x of the quasi-steady field was measured by probes ED4 and ED5, while the component E_z was measured by probes ED3 and ED4 (Fig. 1). The magnetic component $\mathbf{b}_{lf}$ of VLF waves (8 Hz–15.0 kHz) was measured by a separate three-component magnetic detector of the NVK-ONCh complex. The magnetic field components at the AUOS and the subsatellite were measured by SGR-5 and SGR-6 ferroprobe magnetometers with accuracies of 1 nT and 2/16 nT, respectively. (The measurement accuracy of the magnetometer installed at the subsatellite changed automatically, depending on the actual value of the magnetic field **B**.) The electron temperature T_e and the ion density of the thermal plasma $n_i(V)$ (where $0 \le V \le 12$ V is the sweep voltage at the grids of the ion traps) were measured using the KM-10 and KM-13 complexes installed at the station and the subsatellite. (When the plasma is highly perturbed, it is more correct to speak of the ion flux densities along the X and Z directions.) HF wave activity at the *Magion-3* subsatellite was recorded at 198 recording levels in the frequency range 0.1–10 MHz by using a PRS-S receiver with a bandwidth of 50 kHz and threshold sensitivity of 26 dB/μV. The signal was

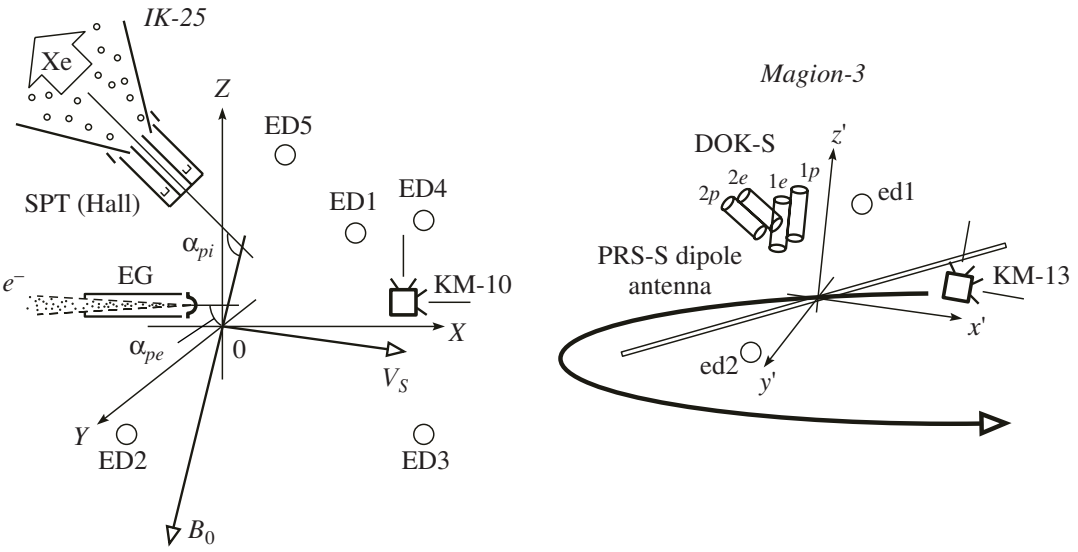

Fig. 1. Injection geometry of the electron beam ($\mathbf{e}^-$) and quasineutral plasma and xenon gas (Xe) and arrangement of the electric field detectors installed at the *IK-25* station (ED1–ED5) and the *Magion-3* subsatellite (ed1 and ed2), the KM-10 and KM-13 complexes for measuring thermal plasma parameters, and the DOK-S spectrometer detectors measuring fast proton ($1p$, $2p$) and electron ($1e$, $2e$) fluxes in the (X, Y, Z) and (x', y', z') coordinate systems of the station and subsatellite, respectively. Here, $\mathbf{B}_0$ and $\mathbf{v}_s$ are the directions of the quasi-steady magnetic field and the station velocity, respectively, and α_{pe} and α_{pi} are the pitch angles of the electron beam and xenon ions injections.

received by a symmetric dipole antenna with a tip-to-tip length of 3 m, and the total HF spectrum of the electric field $\mathbf{e}_{hf}$ was recorded over 0.2 s. A DOK-S charged particle spectrometer installed at the subsatellite measured the differential fluxes of fast electrons and protons in eight energy intervals in the ranges 25–420 and 20–1300 keV, respectively. To record fast particles, two pairs of detectors installed at the subsatellite (detectors $1e$ and $1p$ and detectors $2e$ and $2p$) were oriented in two mutually perpendicular directions. The pitch angles of charged particle injection α_p, the angles of the satellite velocity vector $\mathbf{v}_s$ and the magnetic field $\mathbf{B}_0$, and the angle $\beta_3 \equiv \beta_3(\widehat{\mathbf{B}_0, \nabla Z})$ in the (X, Y, Z) coordinate system (the Z axis is directed along the *IK-25* satellite) were determined using solar and magnetic onboard detectors. The pitch angles α_{p1} and α_{p2} of the fast particles recorded by the DOK-S spectrometer at the subsatellite in the orthogonal directions 1 and 2, the angle ϑ' between the field $\mathbf{B}_0$ and the dipole antenna, and the angle $\beta_1' \equiv \beta_1'(\widehat{\mathbf{B}_0, \nabla x'})$ in the subsatellite coordinate system (x', y', z') were determined using the SGR-6 magnetometer. All the results of component measurements in the satellite and subsatellite coordinate systems (X, Y, Z) and (x', y', z') were recalculated into a new right-handed Cartesian coordinate system (x, y, z ($\vec{z} \parallel \mathbf{B}_0$)) in order to separate out the longitudinal (z) and transverse ($\perp$) components of the vector quantities. Information received during failures of the scientific equipment was marked by a "false" bit, which was common for the entire telemetric frame but was not always actually false for particular devices or measured parameters. To eliminate ambiguity, all the experimental data presented below correspond to the "true" bit only.

In the experiment performed at the 206th turn, the charged particle beams were injected upward, at pitch angles of $\alpha_p > 90°$. The ions were injected in the unmodulated (dc) mode, and the modulation frequency of the electron beam varied every second of the EG operation with pauses of 1 s. Depending on the parameters of injection (such as the power and pitch angle) and beam modulation, different regimes of BPI are possible [6]. For unmodulated electron injection with the flow velocity $u > \omega_\pm/k_z$, the plasma waves grow at a rate γ over the relaxation length $z \sim u/\gamma$. In this case, the electron beam is externally modulated at the frequencies $\omega_\pm$ of hybrid plasma resonances. In contrast, a modulated electron beam suppresses oscillations at all the frequencies except for the modulation frequency ω_m. In this case, due to the slow development of the instability, the relaxation length is larger than that without modulation and the induced spectrum represents a combination of the frequencies ω_m and the BPI spectrum. If the modulation frequency is close to the resonant frequencies of the beam–plasma system, the amplitude of plasma oscillations can increase abruptly. Such oscillations can lead to particle scattering and destruction of the beam system.

The system of an electron beam nested in an ion beam is axially asymmetric with respect to the mag-

netic field direction due to the small velocity of xenon ions ($v_{iz}/u \sim 3 \times 10^{-4}$), which is comparable to the velocity of the satellite ($v_{iz}/v_s \sim 1.5$) moving at an angle to the magnetic field. For certain injection parameters, the generated HF oscillations can reach a saturation level (corresponding to the onset of a nonlinear regime), after which the spectrum begins to extend toward lower frequencies. In this case, the hollow beam of heavy xenon ions injected at pitch angles of up to $\Delta\alpha_{pi} \simeq 60°$ with a maximum flux density within the angles $\Delta\alpha_{pi} \le 30°$ will play the role of a damping layer for waves induced by the electron beam in the entire interaction region in the vicinity of the satellite. In this regard, the generation of extremely low-frequency (ELF) waves and the possibility of controlling the nonlinear interaction mechanism are of most interest. In contrast, since most of the wave energy induced by the ion beam is concentrated in the low-frequency range, we can ignore the influence of low-frequency waves on the HF beam instability at low electron beam currents.

3. MAIN FEATURES OF THE INTERACTION OF AN ELECTRON BEAM WITH THE IONOSPHERIC PLASMA

3.1. When a low-energy electron beam (~10 keV) is injected into the ionospheric plasma, the development of instability and the excitation of electromagnetic fields depend substantially on the shape (current profile) and density of the beam. On the other hand, in a complex current system, the current profile depends on the energy density of the excited waves, which in turn modulate the electron beam, thereby producing a feedback in the beam–plasma system. In order to determine the main characteristics of wave excitation and charge modulation, we assume that the electrons are injected in the presence of induced electric fields (excited over ~1 s), which modulate the beam in the injection region. After several gyrations of dense particle beams, electrostatic repulsion forces transform them into hollow flows with the average density n_{ba} (with $a = e, i$), determined by the expression $I_{ba} \cong 2\pi\int_{r_1}^{r_2} e v_z(r) n_{ba}(r) r dr$, where r_1 and r_2 are the minimum and maximum radii of charged particle gyration at the internal and external boundaries of the beam in a cylindrical coordinate system with $z \parallel \mathbf{B}_0$. The averaged (over the parameter α) flow velocity was determined as $u \equiv \langle v_z \rangle_\alpha = (1/\Delta\alpha')\int_{\Delta\alpha'} v\cos(\alpha_p + \alpha) d\alpha$, where the effective range of pitch angles is $\Delta\alpha' > \Delta\alpha_0$ (about ~2°–3° and ~60° at the injection point $z = 0$ for electrons and ions, respectively). In the case of long injection, the effective range of pitch angles for electrons,

$$\Delta\alpha' \simeq \Delta\alpha_0 + \frac{\pi e}{m v \omega_{ce}} \times (\delta\bar{E}_x + v\delta\bar{B}_z \sin\alpha_{pe} - v\delta\bar{B}_y \cos\alpha_{pe}) \quad (1)$$

reflects the amplitude modulation of the beam by quasi-steady fields in the injection region over a time of $t \sim 1$ s. Here, the upper bar, $\delta\bar{F}_{x,y,z} = \overline{F_{x,y,z} - \bar{F}_{x,y,z}}$, denotes the empirical average over the time interval $\Delta t \sim (7–10)\Delta t_0$, where Δt_0 is the duration of one telemetric frame at the *IK-25* and v is the electron velocity at $z = 0$ (at the output of the EG modulator). The smoothing of the quantities in semiempirical formula (1) is of fundamental importance for eliminating the influence of fast fluctuations on the calculated density of the injected bean; without such a smoothing, numerical instability can arise. The fluctuation amplitudes of the longitudinal and transverse velocities of the injected particles in an equilibrium state and the thermal electron velocity in the flow were estimated using the expressions $\delta v_{r,z} \le \max\{v_{r,z} - \langle v_{r,z}\rangle_\alpha\}$ and $v_{be} \sim (\delta v_z^2 + \delta v_r^2)^{1/2}$, respectively. With a sufficient set of measurement data on the beam and plasma parameters, we can estimate the main characteristics and level of plasma turbulence, as well as the resonant frequencies of the beam and plasma (see table). It should be noted that a considerable amount of compensating electrons with the density n_e and temperature $T_e \sim 3–5$ eV that are ejected from the SPT channel can substantially affect the plasma parameters.

3.2. An inhomogeneous electron beam in the EG chamber is produced in two stages. During short-term ($\tau\omega_m \ll 1$) interaction with the driving field of the modulator, low-energy electrons are first modulated over velocity; then, the beam is additionally accelerated in the space between the anode and the grid modulator, which are at the potentials U_0 and U_1, respectively ($U_1/U_0 \ll 1$). The most important parameters over the length d of the electron–field interaction region are the modulation depth, the change in the field phase, and the efficiency with which the driving field E_1 acts on the beam electrons [7],

$$\xi = \frac{E_1 d}{U_1}, \quad \Theta_1(d) = \omega_m \frac{d}{v_1}, \quad M = \frac{\sin(\Theta_1/2)}{\Theta_1/2}. \quad (2)$$

These parameters determine the electron bunching parameter $X_1(d) = \frac{1}{2}\xi M\Theta_1(d)$ in the modulation space. Assuming that the modulated electric field is much stronger than the beam space-charge field, we find that the electron velocity at the output of the EG modulator is equal to

$$v = v_1\left[1 + \frac{1}{2}\xi M \sin\left(\omega_m t_1 - \frac{\Theta_1}{2}\right)\right], \quad (3)$$

where v_1 and t_1 are the electron velocity at the input to the driving field and the time at which the electron leaves this field, respectively. After the electron beam is ejected from the EG, it soon becomes inhomogeneous due to the difference in the velocities and phases of the

ejected electrons. In order to determine the current $I_{be} = I_0(dt/dt_1)^{-1}$ in the regime of modulation in the simplest case of free electron gyration, it is necessary to find how the time during which electrons travel the distance z depends on the time at which they leave the EG, $t \simeq t_1 + z/v_z$, where v is calculated by formula (3) with the substitution $v_1 \longrightarrow v_0$ (additional electron acceleration in the electrostatic field) and the current I_0 is the beam current at the output of the EG at the first second of dc injection. The electron pitch angle and the bunching parameter over the length z are determined by

$$\Theta_D(z) = \omega_m \frac{z}{v_z}, \quad X_D(z) = \frac{1}{2}\xi M \Theta_D(z).$$

For $X_D \ll 1$, the bunched current is equal to

$$I_{be} \simeq I_0\left[1 + X_D \cos\left(\omega_m t_1 - \frac{\Theta_1}{2}\right)\right].$$

The spectral composition of the current I_{be} is determined by the expression

$$I_{be}(z, t) = I_0 + 2I_0 \sum_{n=1}^{\infty} (-1)^n J_n(nX_D(z)) \times \cos n\left[\omega_m t - \Theta_D(z) - \frac{\Theta_1}{2}\right], \quad (4)$$

where $J_n(nX_D(z))$ is the Bessel function. In the case of 100% modulation ($\xi = 1$), the current profile can be varied by varying the length z in the outer space. The appropriate choice of this length is determined by the relation $Y(t - z/v_z)Y(z) \neq 0$, where $Y(z)$ is the step function. The amplitudes of the harmonics of the convection current are determined by the expression $I^n_{be}(z, t) = 2I_0 J_n(nX_D(z))$. In the regime of modulation, the plasma frequency of the beam electrons ω_{be} is determined for the first harmonic of the convection current, I^1_{be}.

3.3. If we consider only electron injection and assume that the injection of heavy xenon ions does not contribute to the excitation in HF waves (with frequencies on the order of ω_{ce} and ω_{pe}), then the growth rate of quasi-longitudinal waves with frequencies $\omega \simeq \omega_{\pm}(\theta)$ in a "cold plasma–cold beam" system can be determined from the following dispersion relation:

$$1 - \frac{\omega^2_{pe}}{\omega^2}\cos^2\theta - \frac{\omega^2_{pe}\sin^2\theta}{\omega^2 - \omega^2_{ce}} - \frac{\omega^2_{be}\cos^2\theta}{(\omega - k_z u)^2} - \frac{\omega^2_{be}\sin^2\theta}{(\omega - k_z u)^2 - \omega^2_{ce}} = 0, \quad (5)$$

where k_z is the longitudinal component of the wave vector of waves propagating at an angle θ to the magnetic field in the Cartesian coordinate system (x, y, z). If $n_{be} \ll n_0$, then, taking into account that the instability developing at $\omega = k_z u + \epsilon \approx \omega_{\pm}$ and $\epsilon = \delta\omega + i\gamma$ ($|\epsilon| \ll |\omega_{\pm}|$) is absolute in character, we find from Eq. (5) an approximate cubic equation with respect to ϵ. It follows from this equation that, at small detunings, $|k_z u - \omega_{\pm}| \ll \epsilon$, the maximum growth rate is equal to [8]

$$\gamma^h = \frac{\sqrt{3}}{2}\left[\frac{\omega^2_{be}\cos^2\theta(\omega^2_+ - \omega^2_-)\omega_{\pm}}{2|\omega^2_{\pm} - \omega^2_{ce}|}\right]^{1/3}. \quad (6)$$

In the vicinity of the cyclotron resonance $\omega = k_z u - |\omega_{ce}| + \epsilon \approx \omega_{\pm}$ ($|\epsilon| \ll |\omega_{\pm}|$), Eq. (5) transforms into a biquadratic equation, which yields the following expression for the maximum growth rate:

$$\gamma^h = \frac{1}{2}\sqrt{\frac{\omega^2_{be}\sin^2\theta|\omega^2_{\pm} - \omega^2_{ce}|\omega_{\pm}}{|\omega_{ce}|(\omega^2_+ - \omega^2_-)}}. \quad (7)$$

For moderate detunings, when $|\epsilon/(\omega_{\pm} - k_z u)| \ll 1$, or $|\epsilon(\omega_{\pm} - k_z u)| \ll |(\omega_{\pm} - k_z u)^2 - \omega^2_{ce}|$, by linearizing Eq. (5) with respect to the small parameter $\eta = |\epsilon|/\omega_{\pm} \ll 1$ and ignoring the terms on the order of η^3 and η^4, the dispersion relation can be reduced to the form $A\eta^2 + B\eta + C = 0$, where A, B, and C are fairly complicated functions of the parameters ω_{pe}, ω_{ce}, $\omega_{\pm}$, ω_{be}, and v. In this case, the growth rate of the excited waves is equal to

$$\eta = \frac{+\sqrt{|B^2 - 4AC|}}{2A}, \quad B^2 \leq 4AC. \quad (8)$$

Since it is difficult to use Eq. (8) to describe η analytically, we analyzed it numerically in the vicinities of the Cherenkov and cyclotron resonances. When obtaining expressions (6)–(8), it was assumed that the plasma was homogeneous, $\mathbf{u} \parallel \mathbf{B}_0$, and the beam and plasma dielectric constants were defined in the entire space.

The excitation of longitudinal waves with frequencies $\omega = \omega_{\pm} + \epsilon$ in a "cold plasma–warm beam" system at $u > \omega_{\pm}/k_z$ and $\omega_{\pm} \approx k_z u + n|\omega_{ce}|$ (where $n = 0, \pm 1, \ldots$) is described by the expression [9]

$$\gamma^k = -\frac{\sqrt{\pi}\omega^2_{be}\omega_{\pm}}{2k^2 v^2_{be}} \frac{x^{|n|}_{be}}{2^{|n|}|n|!} \times \left[\frac{\omega^2_{pe}}{\omega^2_{\pm}}\cos^2\theta + \frac{\omega^2_{pe}\omega^2_{\pm}\sin^2\theta}{(\omega^2_{\pm} - \omega^2_{ce})^2}\right]^{-1} z_0 \exp(-z_n^2), \quad (9)$$

where

$$z_n = \frac{\omega_\pm - n|\omega_{ce}| - k_z u}{\sqrt{2}k_z v_{be}},$$

$x_{be} = (k_x v_{be}/\omega_{ce})^2$, and the beam electrons obey a Maxwellian distribution.

The most correct interaction model in our case is the "cold plasma–oscillator flow" system in which the beam particles have a finite Larmor radius and large velocity spread along the magnetic field. The growth rates of longitudinal waves in the vicinities of plasma resonances are determined by the expression [10]

$$\gamma^k = -\sum_{n=-\infty}^{\infty} \frac{\sqrt{\pi}}{2}\Omega_{be}^2 \Pi_{ne} \Lambda \omega_\pm \exp(-z_n^2), \qquad (10)$$

where the following notation is used:

$$\Pi_{ne} = z_n J_n^2 + \frac{2n|\omega_{ce}|}{\lambda\omega_\pm} x_{be} y_0 J_n J_n', \quad \Lambda = \frac{|\omega_\pm^2 - \omega_{ce}^2|}{\omega_+^2 - \omega_-^2},$$

$\Omega_{be}^2 = (\omega_{be}/k v_{be})^2$, $J_n \equiv J_n(\lambda)$ is the Bessel function, $J_n' = dJ_n/d\lambda$, $\lambda = k_x v_\perp/\omega_{ce}$, $y_n = (\omega - n\omega_{ce})/\sqrt{2}\,k_z v_{be}$, and $v_\perp$ is the transverse (with respect to the field $\mathbf{B}_0$) component of the velocity. Depending on the parameters, the quantity Π_{ne} at the cyclotron resonance can have different signs in the cases of both the anomalous ($n < 0$) and normal ($n > 0$) Doppler effects. This means that waves can be excited or absorbed over a very wide parameter range and that each particular case should be investigated separately.

3.4. Perturbations of the physical quantities, $\delta\Psi = \{\delta n_{be}, \delta n, \delta \mathbf{v}, \delta\mathbf{E}, \delta\mathbf{B}, \delta T_e, \ldots\}$, with respect to their equilibrium values are defined as $\delta\Psi = \Psi - \Psi^0$, and the equilibrium values of the macroscopic parameters of the beam and plasma are defined as $\Psi^0 = \Psi_0 + \Delta\Psi$, where Ψ_0 denotes the unperturbed quantities and $\Delta\Psi$ denotes perturbations induced by an equilibrium electron beam ($\partial/\partial t = 0$). Small LF and HF harmonic fluctuations averaged over a time $\tau \gg \omega_{ci}^{-1}$, ω_{pi}^{-1}, ω_{pe}^{-1} are zero, $\langle\delta\Psi^{s,f}\rangle_\tau = 0$, and the averaged (over fluctuations) product of two different harmonic quantities $\langle\delta\Psi_1\delta\Psi_2\rangle_\tau \neq 0$ determines the ponderomotive (pumping) action of waves.

3.5. The amplitude of ion-acoustic waves and the level of plasma turbulence as a whole grow under the action of HF oscillations. The levels of Langmuir and ion-acoustic turbulence, $\eta^f \cong W^f/4\pi n_0 T_e$ and $\eta^s \cong W^s/4\pi n_0 T_e$, in the vicinity of the injector determine the dimensions of the turbulence region within which spectral energy is transferred toward shorter wavelengths with the modulation instability growth rate γ_0 when the threshold turbulence level $\eta^f \simeq k_0^2 r_{De}^2$ is reached. When turbulence is so strong that the characteristic scale of plasma pulsations falls into the absorption region, $k_0 \longrightarrow k_* \sim 1/r_{De}$, the ambient plasma is strongly heated. Under our experimental conditions, i.e. at $n_{be}/n_0 \sim (1–5)\times 10^{-3}$ and $v_{be}/v \sim 10^{-2}$–10^{-1}, the relative growth rate of plasma oscillations is $\gamma_0/\omega_{pe} \sim (0.2–0.5)\times 10^{-2}$. When modulational instability increases the amplitude of the HF electric field to the saturation level $W^f \equiv \sum_{\Delta k}\delta E_f(k)^2/4\pi \cong n_{be} m v^2(\gamma_0/\omega_{pe})$ (where $\delta E_f \equiv \mathbf{e}_{hf}$), the entire electron beam–plasma system becomes unstable. This can have a destabilizing effect on electron injection. In [11], a numerical experiment was carried out on the stabilization of BPI in a turbulent plasma with periodic boundary conditions. According to this experiment, stabilization occurs in the nonlinear stage, when the threshold for oscillating two-stream instability is exceeded.

The purpose of the subsequent analysis was to compare the results obtained in experiments performed at the AUOS and the subsatellite with the theory of BPI for different electron beam models during injection of both steady and modulated beams. When comparing the experimental data with numerical results, the presence of a shell of heavy xenon ions was not formally taken into account, although it was assumed that the electron beam could be affected by LF oscillations. It is this circumstance in which our experiment differs from previous ionospheric experiments, although each of those experiments was unique as regard to their conditions and the choice of the beam and plasma parameters.

4. EXPERIMENT ON ELECTRON BEAM INJECTION

When the SPT and EG operated simultaneously and the injection pitch angles differed appreciably from quasi-transverse ones, the thermal distribution of the ion density $n_{ix}(V)$ in a perturbed plasma depended in a complicated manner on the ion composition and ion temperature of the ambient plasma, the electron beam modulation, and the pitch angles α_{pe} and α_{pi}. When the beams were injected in the same direction along the magnetic field, we observed an increase in the total plasma density determined at the *IK-25* from the saturation level $n^0 \equiv n_{ix}$ ($V \leq 1$ V), which satisfied the relation $n^0 = n_0 + \Delta n_{ix}$ (where n_0 is the unperturbed plasma density). This can be seen in Fig. 2, which shows the time dependences of the densities of the perturbed ion flows n_{ix} and n_{iz} propagating in the $-X$ and $-Z$ directions, respectively, and the electron temperature components T_{ex} and T_{ez} measured by the KM-10 device. A sharp increase in density is related to both the release of a neutralizing electron flow with the density n_e from the SPT channel and the specific injection configuration.

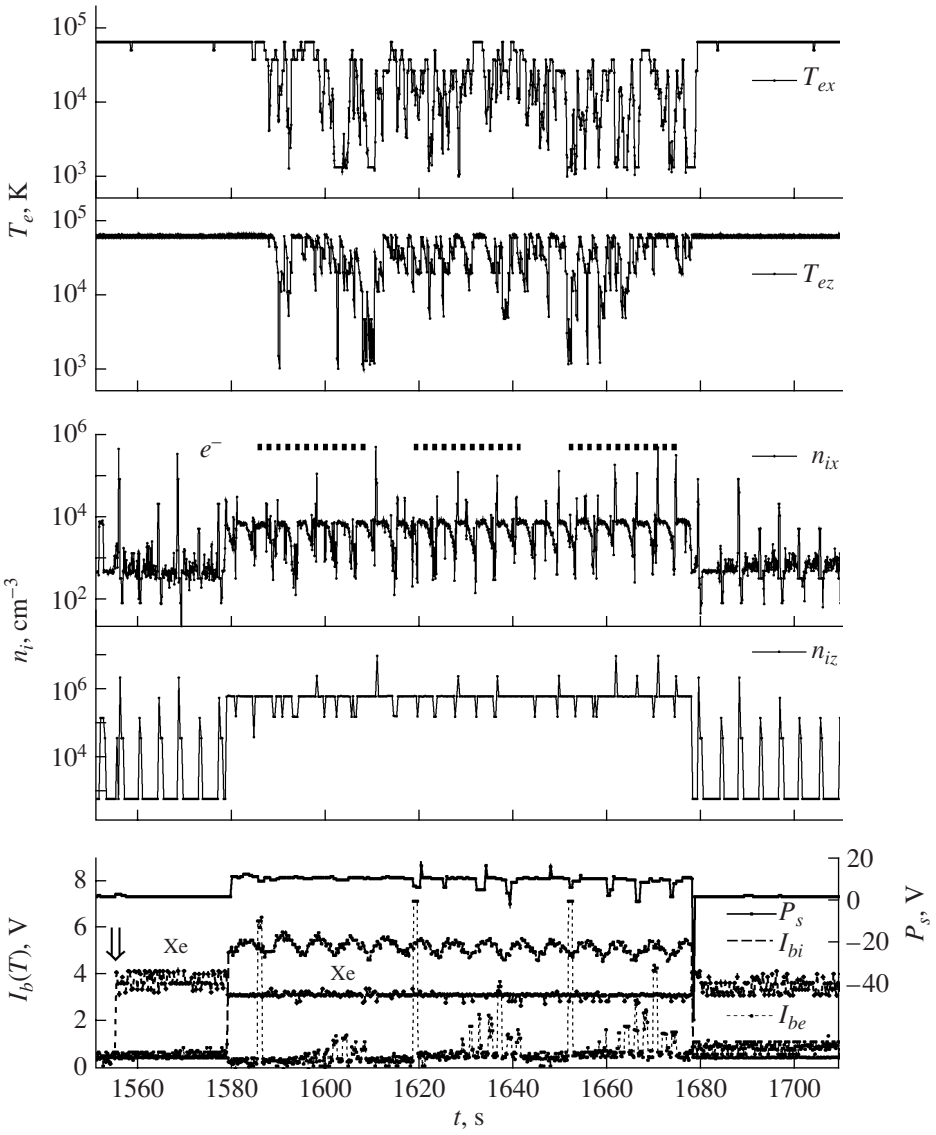

Fig. 2. Time behavior of plasma heating in terms of the longitudinal and transverse electron temperatures, T_{ez} and T_{ex}, and perturbations of the ion flux density of the ionospheric plasma in the *–X* and *–Z* directions at the *IK-25*. The lower plot presents a telemetric record of the injection current I_{bi} of a quasineutral xenon plasma, neutral xenon release (the downward error shows the beginning of release), the UEM electron gun current I_{be} (in telemetric volts), and the potential P_s of the satellite surface. The time t is counted from the instant 3:24:22 UT (before injection), the orbit altitude is H = 1798–1490 km, and the magnetic-shell parameter L is 1.32–1.46. Here and in the subsequent figures, heavy short segments show 1-s intervals (cycles) of electron injection ($\mathbf{e}^-$).

Presumably, the density increases not only in the vicinity of the satellite but over the entire interaction region. In these experiments, the plasma frequency ω_{pe} was determined from the equilibrium value of the density n^0. When the beams were injected in opposite directions, such an increase in n_{ix} was not observed [1]. In contrast, when the retarding potential at the grid of the ion trap during electron beam injection was $V + P_s \gtrsim 10$ V, local variations in $-\delta n_{ix}$ were proportional to the effective angular divergence of the beam in the vicinity of the injector, $\Delta\psi \equiv \cos^3(\alpha_{pe} - \Delta\alpha'/2) - \cos^3(\alpha_{pe} + \Delta\alpha'/2)$. In our case, it is difficult to judge the actual behavior of the plasma temperature (Fig. 2), because necessary conditions for correct temperature measurements were not always satisfied. In [1], experimental results were presented on the increase in the radial temperature component T_{ey} of the ambient plasma for the case of oppositely directed electron and xenon ion beams. According to [1], the radial temperature is proportional to the effective angular divergence in the vicinity of the injector and the velocity spread of the beam electrons, $T_{ey} \sim \Delta v \sim |\Delta\psi|$. The quantity $|\Delta\psi|$ can be regarded as the measure of the quality and heating of the beam propagating through the plasma, because all

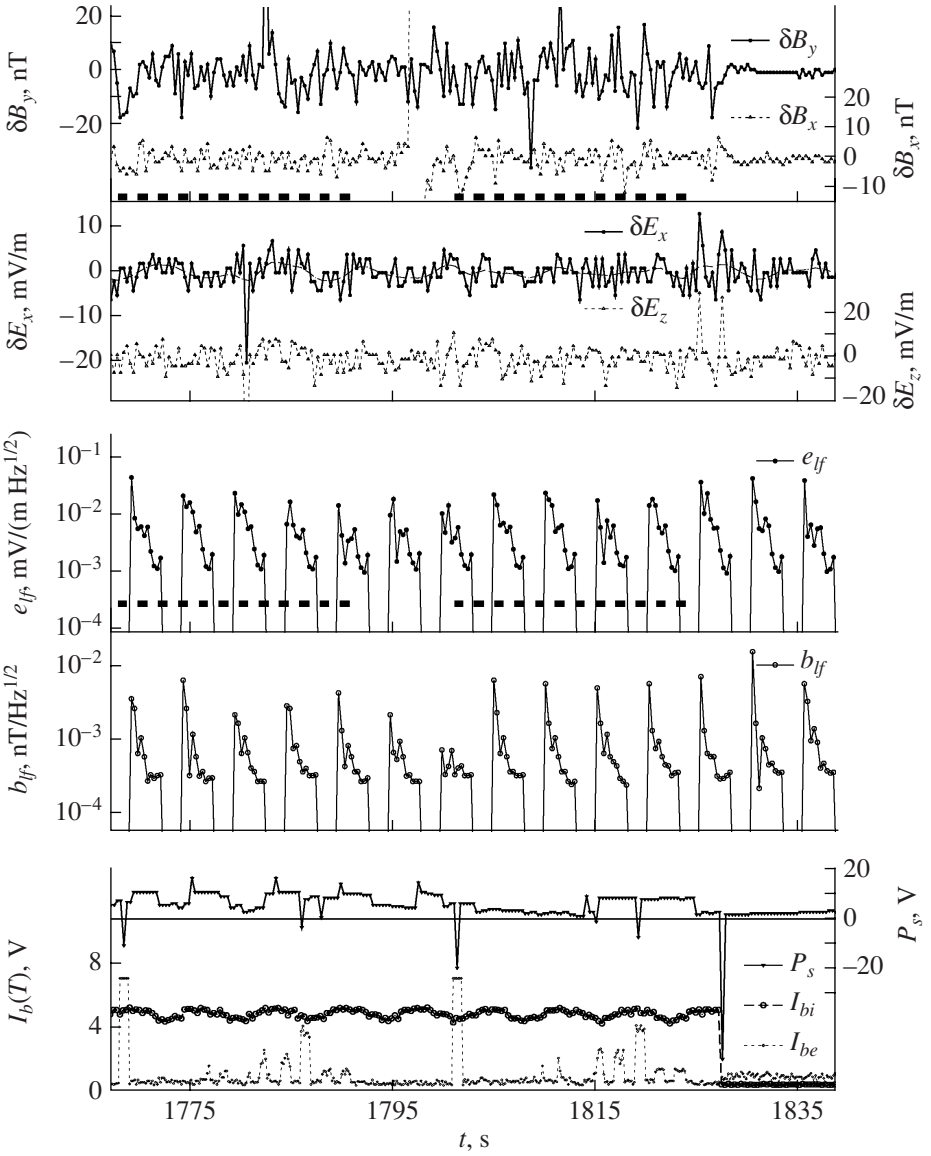

Fig. 3. Time behavior of perturbations of the quasi-steady magnetic and electric fields, $\delta B_{x,y}$ and $\delta E_{x,z}$ (0.1–2 Hz); the spectra of VLF electric and magnetic fields ($\mathbf{e}_{lf}$ and $\mathbf{b}_{lf}$) in the frequency range 8–969 Hz (at ten fixed frequencies); the satellite potential P_s; and the telemetric record of injections at the *IK-25*.

the beam parameters, as well as the development of instability, depend substantially on this parameter. The shape of the electron beam in the vicinity of the injector also depends on the spectrum of the waves that are induced during BPI and propagate back to the injector [12]. The focusing of the beam electrons in electromagnetic fields requires a separate analysis. In calculating the density n_{be} of the injected electrons, we used semiempirical formula (1), which takes into account beam modulation in the vicinity of the injector (see Section 3.1).

Figure 3 shows the time behavior of fluctuations of the quasi-steady magnetic and electric fields, $\delta B_{x,y} = B_{x,y} - \bar{B}_{x,y}$ and $\delta E_{x,z} = E_{x,z} - \bar{E}_{x,z}$ (0.1–2 Hz), measured by DEP-2; the amplitudes of the electric and magnetic fields of VLF waves $\mathbf{e}_{lf} \equiv \mathbf{e}_x$, $\mathbf{b}_{lf} \equiv \mathbf{b}_y$ in the frequency range 8–969 Hz; and the electric potential P_s of the satellite surface. In the initial operation stage of the ion and electron injectors, when the SPT was already switched on but the EG was still inactive, we observed an appreciable increase in electric field perturbations. After the EG was switched on, such perturbations were absent. This effect is presumably related not only to the fact that the beams were injected into the quiet ambient plasma (the release of neutral xenon under conditions of solar illumination began even earlier) but also to the limited capabilities of the two-probe diagnostics, which provides correct measurements of electric fields only in

a weakly perturbed plasma and only at the linear segment of the current–voltage characteristic. Nevertheless, we sometimes observed fluctuations with an amplitude of $\delta E_{x,z} \gtrsim$ 20–30 mV/m and long-period perturbations (synchronous with the injection current of xenon ions) with an amplitude of up to ~5 mV/m (the spline in Fig. 3). Magnetic perturbations with an amplitude of $\delta B_{x,y} \sim$ 10–20 nT, which are related to xenon ion injection [13], rapidly decayed when both injectors were switched off.

The time behavior of the satellite potential P_s during electron injection is similar to that of the negative dc bias of the electrode during the injection of HF power in the plasma. The induced electromagnetic field, once generated, is sustained by electron beam injection, thereby producing a nonlinear pressure on the ambient plasma. This allows us to speak of the pumping effect independently of the type of influence on the ambient plasma, even if it is caused by the beatings of harmonic oscillations of the velocity and density of the electron beam (see Section 3.4). Mechanisms causing a negative bias or, equivalently, the formation of a dc plasma sheath in the vicinity of the satellite during electron beam injection obviously possess their specific features because they depend on the complicated balance of currents in the satellite body. In experiments with an EG carried on the SCATHA geosynchronous satellite, negative pulses of the satellite potential were also observed during the injection of a 3-keV electron beam with a current of 6 mA. An analysis of the data from the analyzer of the satellite electric charge showed that these pulses were accompanied by electric discharges at the satellite; as a result, two detectors became disabled [4]. In our case, a more intense injection did not have any negative effect on the scientific equipment; this was also proved in a more complicated experiment with asynchronous injections at the 277th turn [1, 2]. The role played in these processes by the injection of the compensated ion flow and xenon gas jet is also of interest.

It is worth noting the following results obtained in experiments in which the electron and ion beams were injected in the same direction (see Figs. 2, 3).

(i) An increase in the intensities of the ion plasma components (plasma density) was observed during the injection of a compensated xenon ion flow ($n^0 \sim n_{bi}$).

(ii) An increase in the amplitudes of the electric and magnetic components of ELF waves (8–33 Hz), e_{lf} and b_{lf}, was observed during the first several seconds of xenon ion injection and in pauses between injection pulses. The parameters of waves in this frequency range are also highly sensitive to modulated electron injection.

(iii) During dc electron injection, as well as during injection modulated at frequencies of $\omega_m \geq$ 62.5 kHz, negative pulses of the satellite potential with an amplitude of $\delta P_s \sim$ 10–20 V were recorded.

Figures 4–6 present data from measurements of HF fields by the PRS-S receiver installed at the subsatellite, which was somewhat aside from the magnetic tube, at a distance of ~120 km from the station. Figure 4 shows the time behavior of the HF field amplitudes $\mathbf{e}_{hf}$ at the frequencies $f = \omega/2\pi$ = 0.40, 0.45, and 0.85 MHz; the injection pitch angles; the orientation angles ϑ' and β_1' of the dipole antenna of the PRS-S receiver; the magnetic field $\mathbf{B}_0$ in the subsatellite coordinate system; and the calculated values of the injection density and instability growth rate for flows of oscillators with a large spread in longitudinal velocities of the beam particles [10]. The density n_{be} during modulated injection was estimated from the first harmonic of the convection current $I_{be}^1 = 2I_{be}J_1(X_D(z))$ at z = 1000 m and the effective value of the initial electron bunching, ξ' = 0.75 (75% amplitude modulation) and $\Delta\alpha_0 = 2.5°$. The time dependence of the density in the ac mode is very close to the telemetric current profile shown in Figs. 2 and 3. However, the density can be estimated only indirectly, by fitting the parameters of electron bunching and modulation in the UÉM chamber (see Section 3.2). Note that pauses in the operation of the equipment installed on the *Magion-3* subsatellite ($t \cong$ 1571–1623 and $t \cong$ 1719–1772 s) are not related to the active operation cycles of the *IK-25* and are caused by purely technical reasons. Unfortunately, these pauses did not allow us to study processes that occurred far from the injection region in the initial stage of an active operation cycle. We can assert, however, that spikes of HF radiation at the resonant frequencies $\omega \sim \omega_\pm$ are related to modulated electron injection ($\omega_m \geq$ 15.625 kHz) and the relaxation of the plasma channel after the wave and electron–beam pumping are terminated. Although the EG operated at a power level of 90%, spikes of HF radiation were sometimes absent. Figure 5a shows the HF spectra of the signal from the PRS-S receiver at the instant *A* indicated in Fig. 4. The spectra demonstrate a considerable increase in the wave intensity near the frequencies ω_- and ω_{pe}, followed by energy transfer (over ~0.3–0.4 s) to the long-wavelength part of the spectrum during the decay of strong turbulence. Such an abrupt increase in the intensity of HF waves in the plasma (the SPT is not yet switched on, although neutral xenon has been released several seconds earlier) and correlation with the subsequent breakup of the scientific equipment are difficult to explain. Spectra shown in Fig. 5b were recorded at the 8th and 9th seconds of injection, the modulation frequencies being $\omega_m/2\pi$ = 15.625 and 31.25 kHz, respectively, which, for hydrogen-like plasma, are slightly lower and larger than the ion plasma frequency $\omega_{pi}/2\pi \sim$ 16–17 kHz. Due to the contribution from the heavier ion components, the effective frequency ω_{pi} is shifted toward lower frequencies and is very close to the plasma frequency of the beam electrons; i.e., in this case, we can speak of the double resonance $\omega_m \sim \omega_{pi} \sim \omega_{be}$. The presence of a signal at frequencies close to the

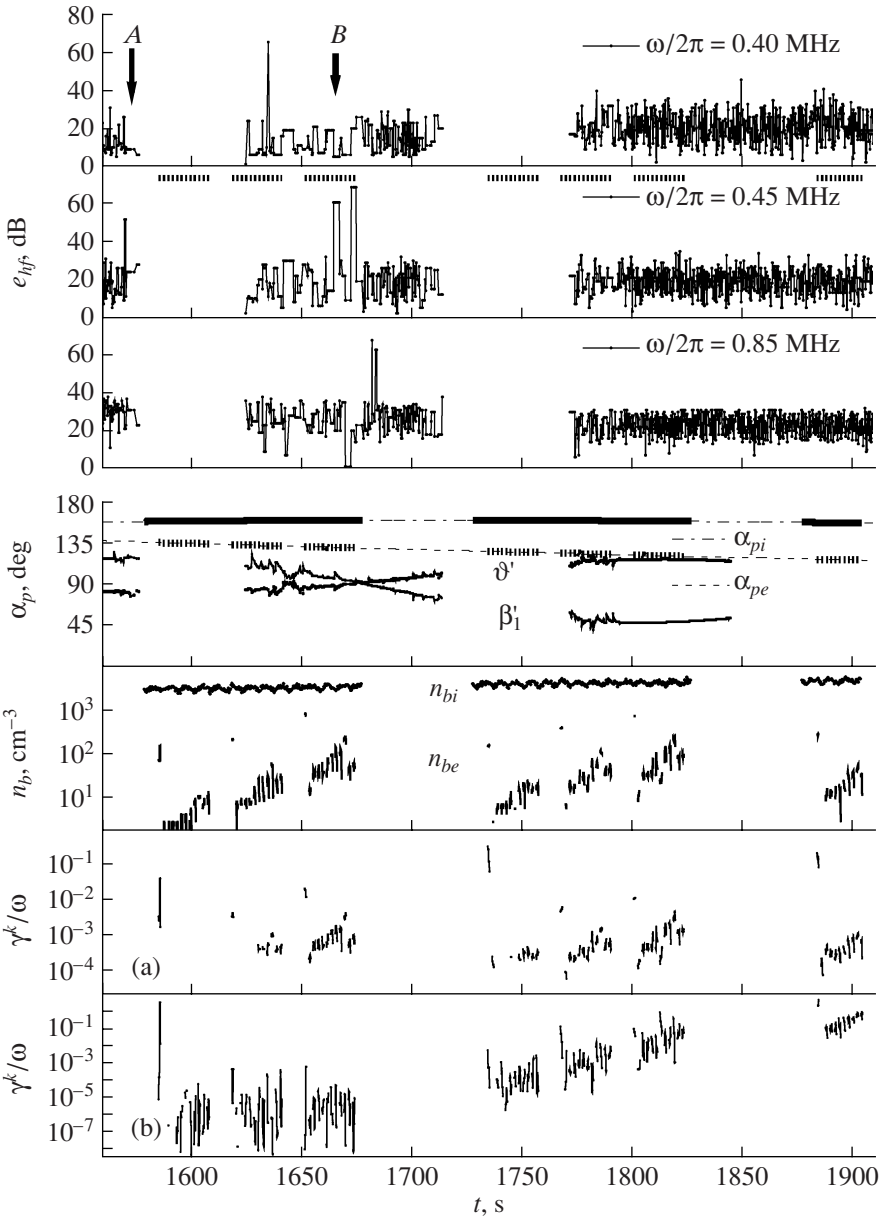

Fig. 4. Time evolution of the HF field amplitudes e_{hf} at the frequencies $\omega/2\pi = 0.40$, 0.45, and 0.85 MHz, recorded by the PRS-S receiver at the *Magion-3* subsatellite during an active operation cycle. The lower plots show the pitch angles of xenon plasma and electron beam injection (the dashed lines with heavy solid segments indicate the instants of injection); the angles β'_1 and ϑ' between the magnetic field and the x' axis and the PRS-S dipole antenna, respectively, in the subsatellite coordinate system; and the calculated values of the beam densities n_{be} and n_{bi} and the relative growth rate γ^k/ω_- of kinetic instability in the "cold plasma–oscillator flow" model [10] for the $\omega = \mathbf{k}\cdot\mathbf{v} + n|\omega_{ce}|$ resonances: (a) $\theta = 0.04$, $n = 0$ and (b) $\theta = 0.64$, $n = -1$.

electron plasma frequency when the pumping (electron beam modulation) is performed at frequencies close to ω_{pi} is quite natural, because the wave pumping into ion-acoustic turbulence via modulational instability leads to an increase in the number of plasmons (see Section 3.5). An increase in the wave amplitude in the vicinity of the plasma resonance ($\omega_m \approx \omega_-$ ($\theta \neq 0$) cannot be attributed only to the trivial resonant mechanism of wave excitation, $\sim(\omega + \epsilon - \omega_-)^{-1}$, because small detuning from the resonant frequency, $\Delta\omega = \omega_- - \omega$, assumes that the values of $\mathrm{Re}\,\delta\omega$ and γ are anomalously large, i.e., that not only the increase in wave amplitude is large but also that the resonance conditions are violated when the frequency is shifted by $\mathrm{Re}\,\delta\omega$.

The main results of the subsatellite HF measurements can be formulated as follows:

(i) the modulation of the electron beam at frequencies that are far from the resonant frequencies of the

beam or plasma leads to the suppression of HF perturbations in the range of resonant frequencies ω_{pe} and ω_{ce},

(ii) the data from the PRS-S receiver (partially presented in Figs. 4 and 5) indicate that the amplitude of HF waves increases during the injection of an electron beam modulated at a frequency of $\omega_m \gtrsim \omega_{pi}$, and

(iii) an increase in the amplitude $\mathbf{e}_{hf}$ at frequencies $\omega/2\pi \sim 0.25$ MHz is observed after the 12th second of electron injection (similar retarding phenomena in the HF range were observed in the *Polar-5* experiment [3]).

In order to reveal new regularities in the growth rates of longitudinal waves excited via the (a) Cherenkov and (b) cyclotron resonance mechanisms (see Fig. 4), it is necessary to perform an additional analysis of the experimental results.

Figure 6 shows the time dependences of the differential fluxes of fast electrons and ions (primarily protons) recorded in directions 1 and 2 (see Fig. 1). The time dependences of the corresponding pitch angles are shown in the lower plot. These results (as well as those presented in Figs. 2–4) are rather difficult to analyze; nevertheless, we can assert that spikes of the differential fluxes of fast particles are caused by electron injection from the main satellite. This concerns not only the enhancement of fluxes due to the acceleration of charged particles in the field of potential or electromagnetic waves, but also the occurrence of suddenly weakened, scattered fluxes of fast electrons (negative spikes) when passing through the regions of strong turbulence in the ionosphere [14]. Figure 7 shows the energy spectra of the particle fluxes, $J_{e,p}^{\max}$ and $J_{e,p}^{\min}$, measured at instants *C* and *D* indicated in Fig. 6. These spectra correspond to the injection of an electron beam modulated at the frequency $\omega_m/2\pi \sim 0.125$–0.25 MHz and to a pause between the 60% and 90% injection powers, respectively. In the spectra measured at instant *C*, the fluxes of electrons moving at very small pitch angles have two maxima in the range of low energies (near 25 and 100 keV) and one maximum (at $\alpha_{p2} \simeq 70°$–$76°$) near 180 keV. The occurrence of low-energy electrons can be attributed to the excitation of HF waves and the interaction at the harmonics $k_z u - n|\omega_{ce}|$ ($n = 0, \pm1, \pm2, \ldots$), whereas anomalous fluxes of fast ions can arise only due to the interaction with VLF waves. Note that conditions for the direct excitation of low-frequency electromagnetic waves by the electron beam are far from optimal, because, for the velocity ratio $(v_A - u)/v_{be} \sim -(20$–$30)$, the growth rate of VLF electromagnetic instability is lower than the damping rate of Alfvén waves [15].

The spectra measured at instant *D* could be regarded as unperturbed ones if there were no dc injection of heavy xenon ions capable of exciting VLF waves or if Alfvén waves could not be excited at the instant when electron injection was switched off. In any case, both the enhancement and suppression of ion fluxes are observed in the ion spectra in the energy range $\varepsilon_p \gtrsim$ 660 keV. The particle fluxes in Fig. 6 demonstrate similar behavior after both the electron and ion injectors are switched off. Indirect evidence of the retarded precipitation of electrons with energies one order of magnitude higher than the energy of the injected electrons (0.5 A, 27 keV) was previously observed in the *Araks* rocket experiment. Later, X-ray bursts observed in the *Trigger* experiment were also attributed to the precipitation of fast particles [4, 16]. Figures 6 and 7 present one of the first direct proofs of the existence of mechanisms for the generation of fast electrons and ions after the end of injection due to the passage of induced VLF waves along the ionospheric waveguide. In our experiments, spikes of anomalous fluxes of fast particles during electron injection were observed for the first time. The question however arises as to the influence of the

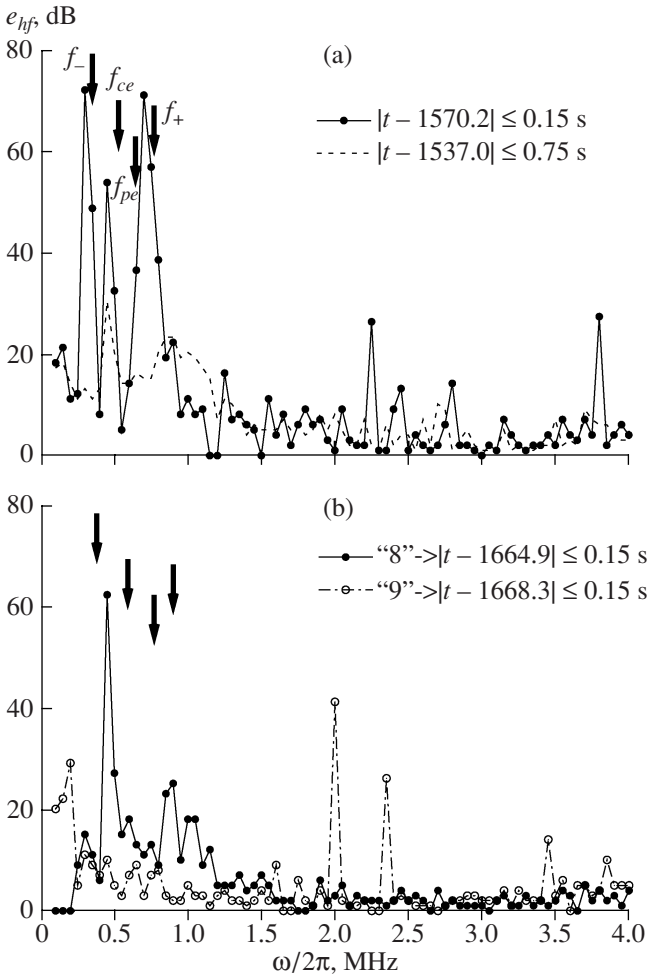

Fig. 5. HF spectra of the received signal at the *Magion-3* in the frequency range 0.1–4.0 MHz for instants (a) *A* and (b) *B* in Fig. 4. The vertical arrows indicate the hybrid ($\theta \approx 0.64$), electron cyclotron, and plasma frequencies ($f_\pm$, f_{ce}, and f_{pe}, respectively). The dashed line in plot (a) shows the unperturbed HF spectrum, averaged over a 1.5-s time interval. The "8" and "9" spectra presented in plot (b) correspond to the eighth and ninth seconds of electron injection.

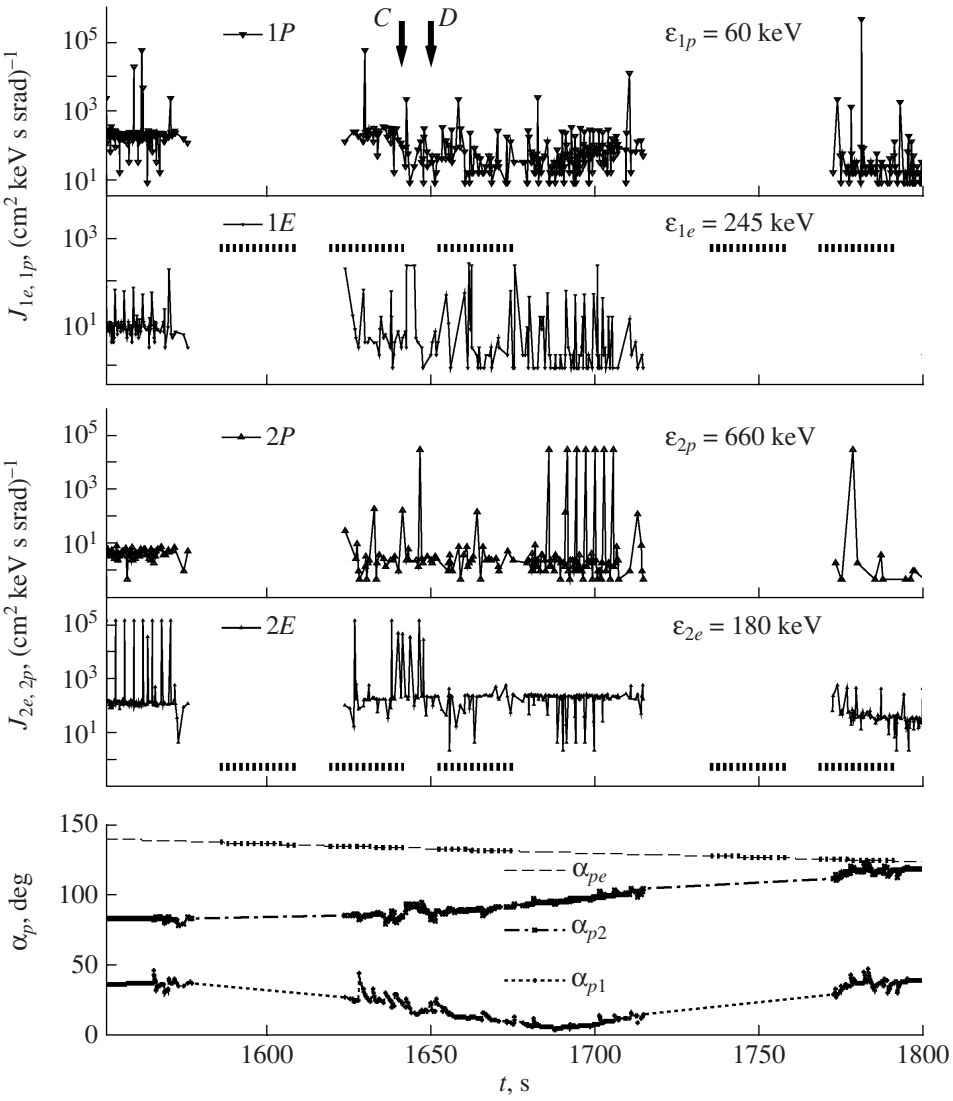

Fig. 6. Time evolution of the differential fluxes of fast ions and electrons recorded in mutually perpendicular directions "1" and "2" in the active segment of the 202th turn (on top) and the pitch angles of electron injection (α_{pe}) and charged particle recording (α_{p1} and α_{p2}) at the *Magion-3* (on bottom).

injected ions and the injection configuration as a whole on the acceleration mechanisms.

The results concerning the interaction of the excited waves with the ionospheric plasma particles can be briefly summarized as follows:

(i) the generation of resonant (anomalous) electron fluxes in the energy ranges 25–30 and 100–200 keV is directly related to the excitation of HF waves during the injection of an electron beam with a power of ~1 kW,

(ii) the spikes of fast ~1-MeV ion fluxes can be attributed to the generation of ELF Alfvén waves during the injection of an electron beam through a beam of heavy xenon ions, and

(iii) the retarded precipitation (scattering) of fast ions and electrons after the end of both electron and ion injection agrees with the results of the *Araks* and *Trigger* experiments.

The time dependences of the measured and calculated parameters presented in Figs. 2–4 and 6 do not allow one to thoroughly analyze the development of perturbations under conditions of fast alternating processes. In analyzing new dependences on an arbitrary parameter p (see Figs. 8–11), the measured and calculated parameters of spatiotemporal processes, h_i and s_i, were transformed (with allowance for simulations of active space experiments) into a new sequence, $h_i(t)$, $s_i(t)$, $p(t) \Rightarrow h_i(p)$, $s_i(p)$, in ascending order of the parameter p. All the transformations preserve the structure of the data set $\{h_i, s_i\}$, which forms a separate physical record as an event characteristic. Such a change of variables provides a more illustrative repre-

sentation of the processes and allows one to reveal specific features of the experimental results. Figure 8 shows the wave growth rates γ^k for the Cherenkov resonance at $\omega \gtrsim \omega_-$ as functions of the parameter $p \equiv p_1 = \omega_{be}^2/(\omega_r^2 - \omega_{ce}^2)$, where $\omega_r = \omega - k_z u$. The growth rate γ^h for waves with the frequencies $\omega \lesssim \omega_-$ was also estimated using hydrodynamic theory (see Eqs. (6)–(10)). The kinetic and hydrodynamic growth rates were calculated for the same value of the detuning $|\Delta\omega|$. The upper plot in Fig. 8 shows the growth rate γ^h calculated by formula (8).

Note that the calculated growth rates are very sensitive to small variations in the ionospheric parameters the data on which are supplied in the real-time mode to the input of the numerical algorithm for determining the parameters of instability. The optimal choice of the parameter p allows one to find the relation between the experimental results and BPI instability, provided that this instability is a dominant interaction mechanism. The absolute character of BPI implies that the larger the growth rate, the larger the amplitude of the excited HF waves at all the spatial points reached by the perturbation. This direct relation makes it possible to estimate the effect of instability; all the other experimental results can only be regarded as indirect consequences of BPI. The upper plot in Fig. 8 shows the factors (numerical parameters) Ω_{be}^2 and $\Lambda\omega_-$, which actually determine the kinetic growth rate. The HF field amplitude e_{hf}, the fast electron flux J_e, and the quasi-steady magnetic field perturbations ΔB_x recorded at the *Magion-3* at some values of p_1 correlate with the growth rate γ^k and the parameter Λ. It was also found that the perturbations δB_x, the electron flux, and the growth rate γ^k at $p_1 \simeq -0.2$ are correlated with one another. For $p_1 \gtrsim -0.1$, a similar correlation was also observed experimentally; in this case, however, such a correlation was not caused by the onset of BPI only. The governing factors in the development of BPI are the resonance detuning $|\Delta\omega|$; the beam density n_{be}; and velocity v_{be}, which characterizes the efficiency of beam heating. Since the determination of each of these quantities encounters difficulties, the observed disagreement between the experimental results and the absolute character of instability does not always contradict to Cherenkov interaction mechanism. It should also be taken into account that, over a time of $\tau \sim 1/\gamma$, the resonance detuning $|\Delta\omega|$ changes by a value equal to the frequency shift $|\delta\omega|$ of the plasma resonance in the presence of a beam. This makes instability a hardly detectable phenomenon during slow telemetry. The density of the injected electrons in the modulation mode was calculated for the first harmonic of the convection current I_{be}^1 with a number of simplifying assumptions, among which the estimate of beam heating by the formula $v_{be} \sim \Delta v \equiv \max\{\delta v\}$ seems to be the most correct.

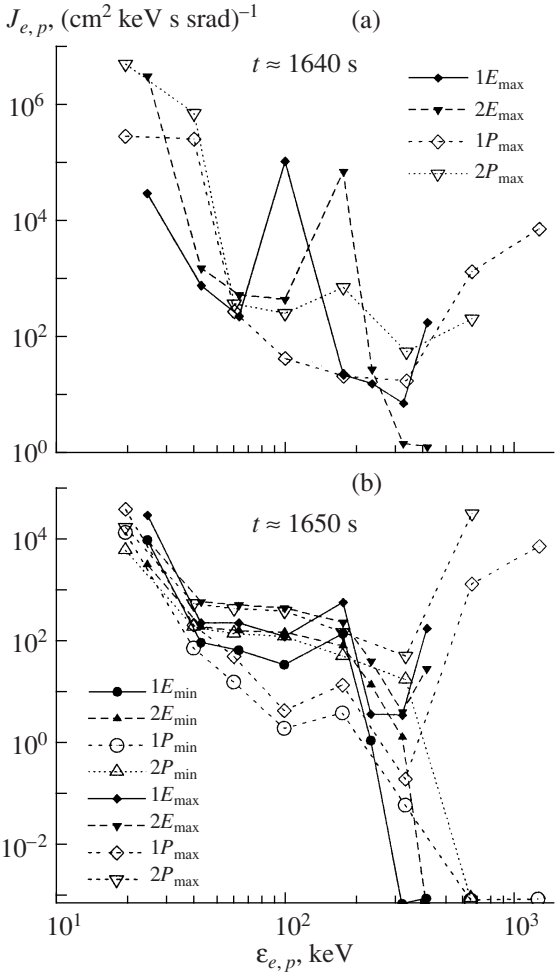

Fig. 7. Spectra of the maximum and minimum fluxes of fast particles at instants (a) *C* and (b) *D* (see Fig. 6), measured at $\alpha_{p1} \simeq 17°$–$25°$ and $\alpha_{p2} \simeq 68°$–$76°$ in the electron energy range 25–420 keV and proton energy range 20–1300 keV.

The upper plot in Fig. 9 shows the growth rates $\gamma^k(p_1)$ for the Cherenkov resonance at different values of the detuning $|\Delta\omega|$ and the beam heating v_{be}. For comparison, the figure also shows the hydrodynamic growth rate $\gamma^h(p_1)$, described by Eq. (6) [9], and the velocity spread Δv of the beam electrons. The experimental results are presented by the data on perturbations of the quasi-steady electric and magnetic fields, δE_x and δB_y, and the amplitude of the magnetic component of VLF waves at the frequencies $f = 9.6$ kHz and 33 Hz, recorded at the *IK-25*. Although the values of beam heating ($v_{be} \simeq 0.35\Delta v$ and $\simeq 0.75\Delta v$) and detuning $|\Delta\omega|$, which are used to estimate the BPI growth rate, differ insignificantly in these two cases, variations in γ^k behave in different ways. During injection, the time behavior of the perturbed field δE_x is similar to that of Δv and is partially similar to γ^k (for $v_{be} \simeq 0.35\Delta v$), although there is no direct relation with the mechanism of HF instability. Obviously, electric

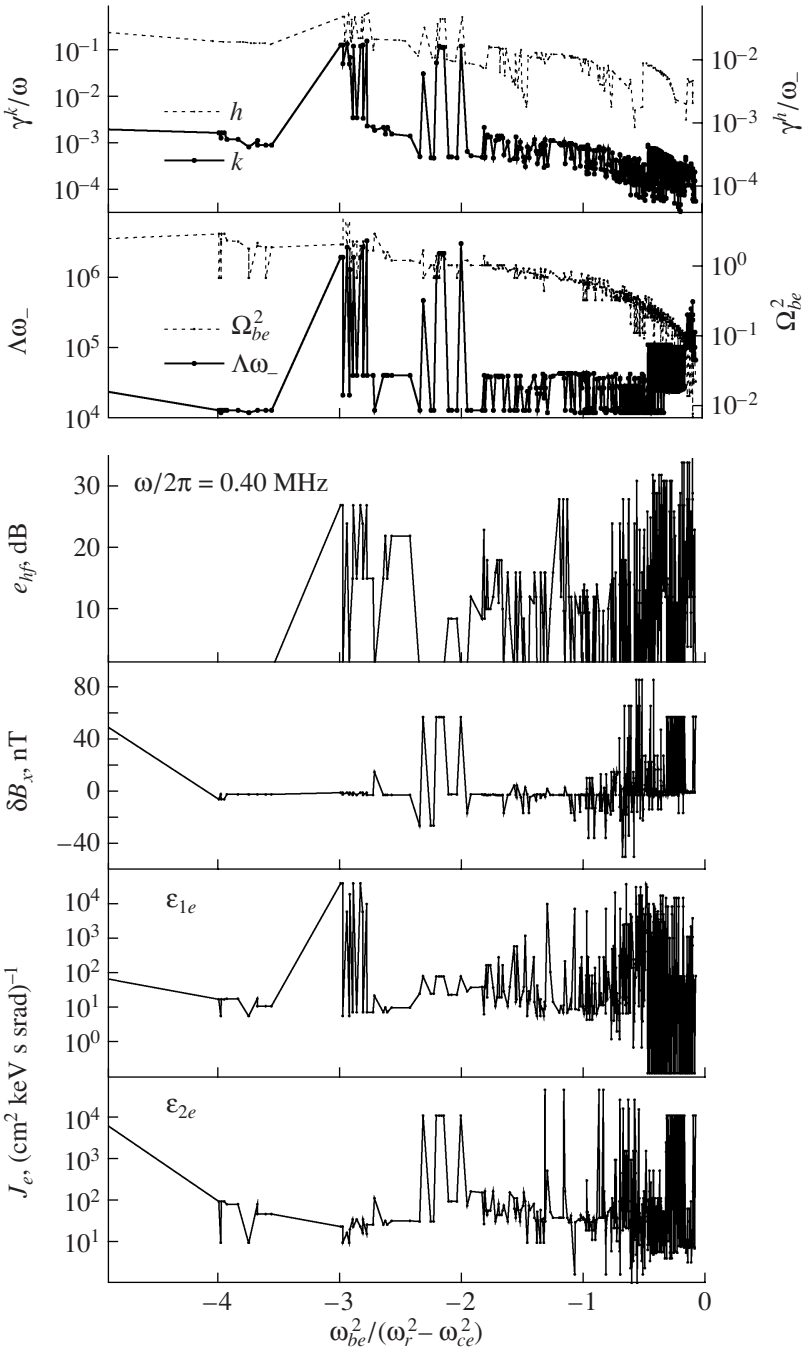

Fig. 8. Normalized growth rates of the kinetic [10] and hydrodynamic (8) BPI ($\gamma^k(p)$ and $\gamma^h(p)$) in the frequency range $\omega \sim \omega_-$ for the $\omega = \mathbf{k} \cdot \mathbf{v}$ resonance ($n = 0$) at angles of $\theta \simeq 0.04$ (see Fig. 4a), parameters Ω_{be}^2 and $\Lambda\omega_-$, measured amplitudes of the HF electric field at the frequency 0.40 MHz, and fluctuations of the quasi-steady magnetic field and 101-keV electron fluxes measured in two mutually perpendicular directions "1" and "2" at the *Magion-3* subsatellite as functions of the parameter $\omega_{be}^2/(\omega_r^2 - \omega_{ce}^2)$.

field perturbations are electrostatic in character and $\delta E_x \sim \Delta v \sim \Delta\psi$, which confirms the conclusions of [1]. Magnetic perturbations are presented in the figure by VLF waves in the frequency ranges 9.6 and 33 kHz ($b_{9.6}$ and b_{33}, respectively) and by δB_y (which is comparable with p_c1 pulsations).

Along with perturbations similar to δE_x, the behavior of magnetic perturbations in the range $10^{-2} \lesssim p_1 \lesssim 10^{-1}$ is also of interest. In this range, a pronounced maximum of the VLF component $b_{9.6}$, the suppression of the ELF wave amplitude b_{33}, and appreciable (~60 nT) short-period (fractions of a second) pulsations of δB_y

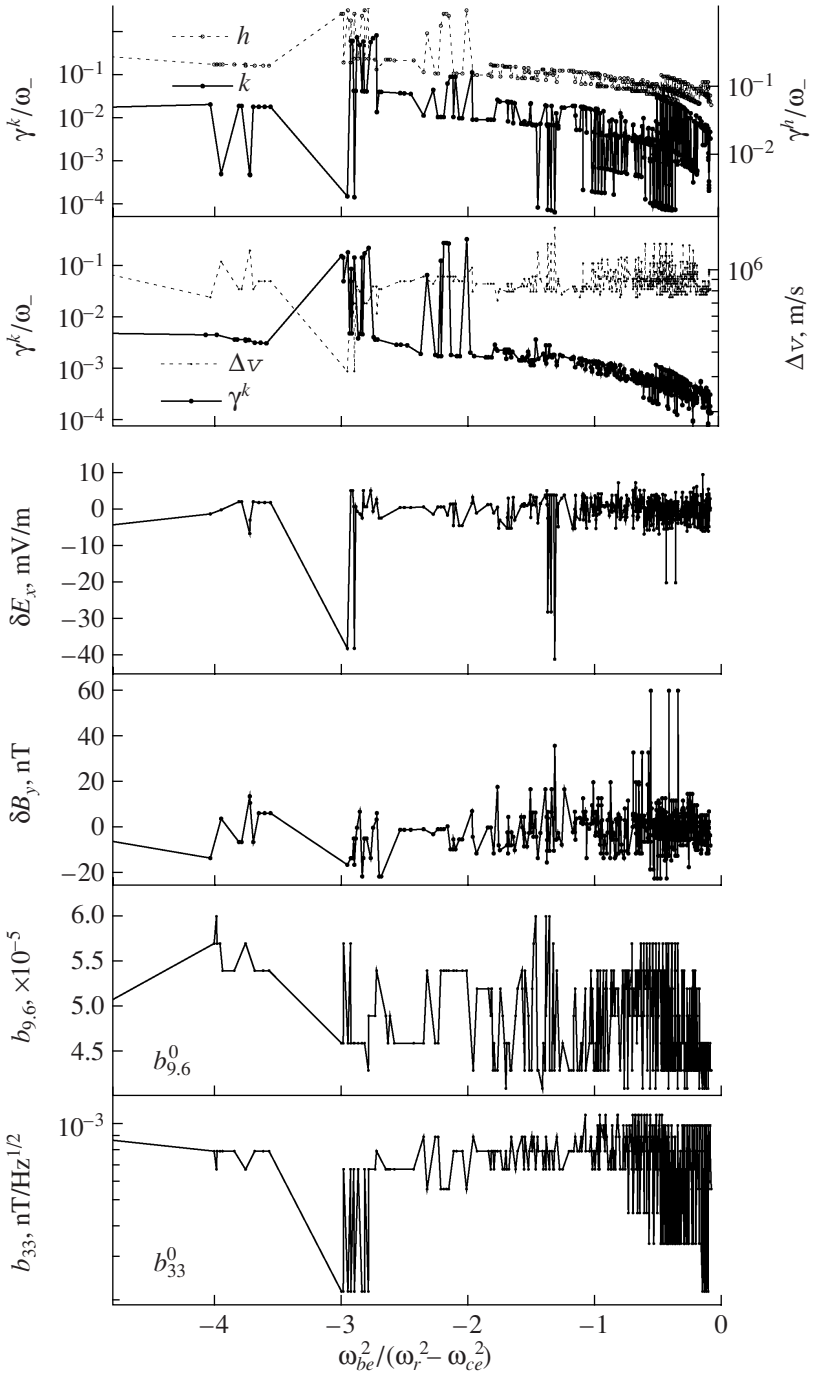

Fig. 9. Two versions of the development of kinetic instability in the "cold plasma–oscillator flow" model for the detuning $\Delta\omega \approx 0.15\omega_-$, $\theta = 0.04$, and $n = 0$ at $v_{be} \simeq 0.35\Delta v$ (the upper plot) and $v_{be} \simeq 0.75\Delta v$ (the second plot), hydrodynamic growth rate γ^h (6) for $\omega \lesssim \omega_-$, and electric (δE_x) and magnetic (δB_y) components of the VLF field measured at the *IK-25* at the frequencies 9.6 kHz and 33 Hz as functions of the parameter $\omega_{be}^2/(\omega_r^2 - \omega_{ce}^2)$. The amplitudes of magnetic perturbations $b_{9.6}$ and b_{33} shown in the two lower plots correspond to the resonance between the plasma frequency of the beam electrons and the lower hybrid frequency of the ionospheric plasma.

are observed. These perturbations are probably related to the resonance between the plasma frequency of the beam electrons and the lower hybrid frequency of the ambient plasma, $\omega_{be} \sim \omega_{LH} \equiv \omega_-(\theta = \pi/2)$, or the Langmuir frequency of the background ions (primarily protons), $\omega_{be} \sim \omega_{pi}$. The less probable mechanism in this case is the resonance between the modulation frequency ω_m and the frequencies ω_{LH} (ω_{pi}), because spe-

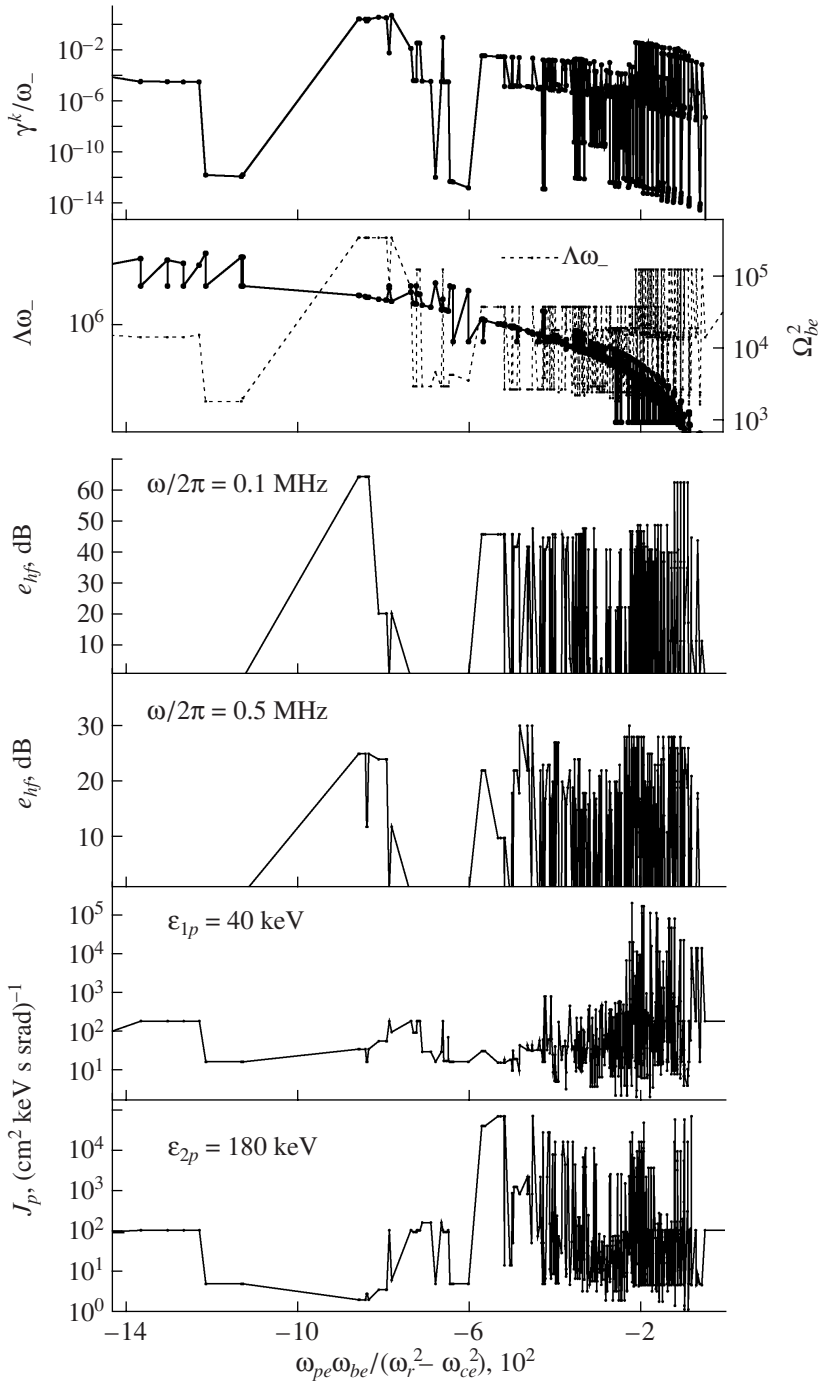

Fig. 10. Instability parameters $\gamma^k(p)/\omega_-$, Ω_{be}^2, and $\Lambda\omega_-$ for the flow of oscillators at $\theta = 0.64$, $n = -1$, and $\Delta\omega \simeq 0.25\omega_-$ (Fig. 4b); HF field amplitudes; and differential fluxes of fast ions with the energies $\epsilon_{1p} = 40$ keV and $\epsilon_{2p} = 180$ keV, measured in two mutually perpendicular directions, as functions of the parameter $\omega_{pe}\omega_{be}/(\omega_r^2 - \omega_{ce}^2)$.

cial analysis showed that the modulation frequency was distributed irregularly with respect to p_1. In contrast, the ratio ω_{be}/ω_{LH} gradually decreases to ~1 in the range $p_1 \gtrsim -0.1$ (Fig. 9). For a hydrogen plasma, the lower hybrid frequency is equal to $\omega_{LH}/2\pi \simeq 11$ kHz; this value may be slightly overestimated because of the presence of a small admixture of heavier ions. Therefore, in this case, it is reasonable to speak of the resonance between the Langmuir frequency of the beam electrons and one of the plasma frequencies (ω_{LH} or ω_{pi}). In [2], the excitation of VLF waves and magnetic field fluctuations with an amplitude of $|\delta\mathbf{B}| \sim 100$–

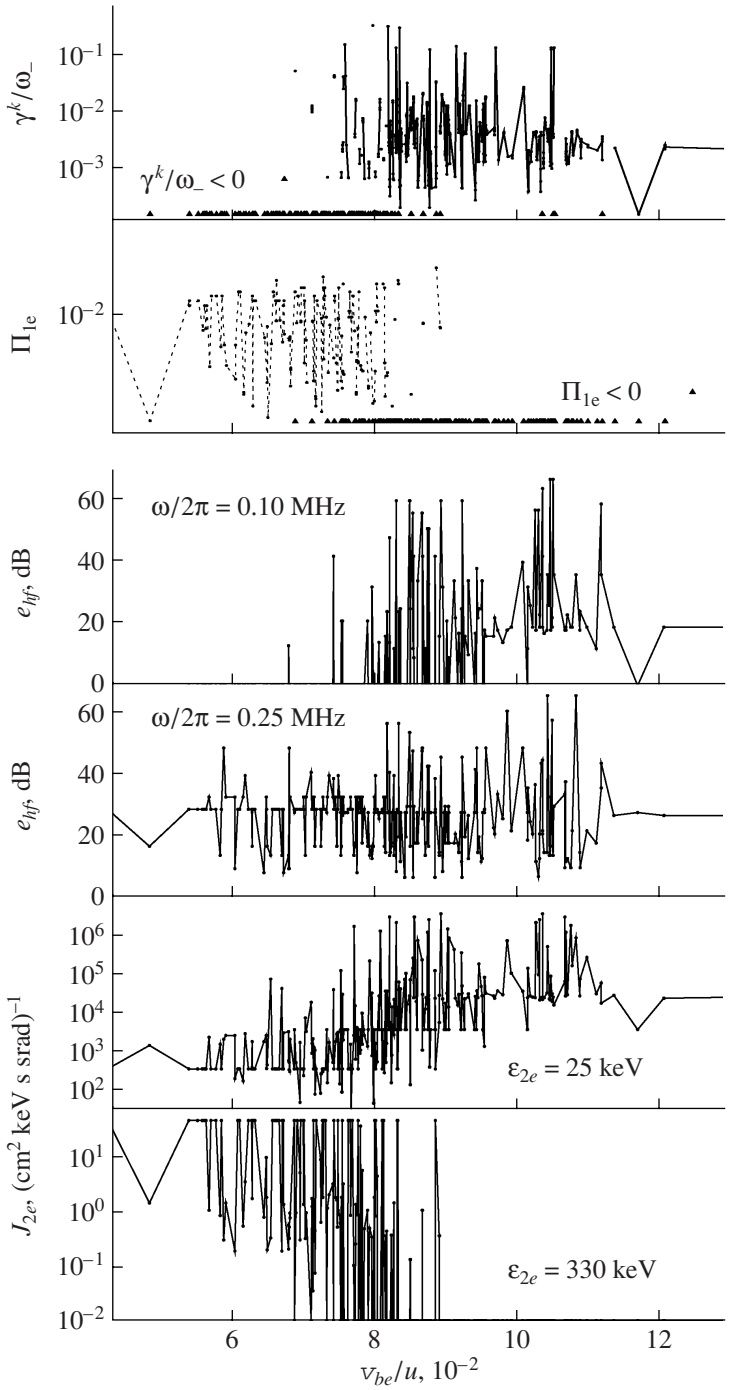

Fig. 11. Growth rate γ^k and polynomial Π_{1e} (for $\theta \simeq 0.64$, $\Delta\alpha_0 \approx 1.5°$, and $\xi' = 0.85$) [10], HF field amplitudes, and fluxes of fast electrons as functions of the relative beam heating v_{be}/u. The inequalities $\gamma^k > 0$ ($\Pi_{1e} < 0$) and $\gamma^k < 0$ ($\Pi_{1e} > 0$) correspond to the excitation and damping of HF waves, respectively.

500 nT was attributed to the nonlinear generation of currents and the operation of the dynamo mechanism in the plasma during electron beam injection with the flow velocity $\mathbf{u} \simeq \mathbf{v}_A$ (the Alfvén resonance). On the whole, the experimental results recorded at two remote spatial points are unambiguously related to electron injection and those recorded at the *Magion-3* can be partially related to the onset of BPI at the Cherenkov resonance.

Let us briefly formulate the intermediate conclusions:

(i) due to the excitation of longitudinal HF waves by the electron beam, anomalous fluxes of 100-keV elec-

trons are observed far from the injection region (at the subsatellite),

(ii) the induced HF instability is accompanied by the generation of VLF waves and large-amplitude magnetic field fluctuations (Alfvén waves), and

(iii) the resonance excitation of lower hybrid waves at $\omega_{LH}/\omega_{be} \longrightarrow 1$ and the suppression of ELF waves in the frequency range $\omega \lesssim \omega_{ci}$ are observed at electron beam densities as low as 1–3 cm^{-3}.

Figures 10 and 11 illustrate the parameters of kinetic instability against the excitation of nearly longitudinal waves at the cyclotron resonance $n = -1$ for the "cold plasma–oscillator flow" model. The growth rate $\gamma^k \equiv \gamma_n^k$ (see expression (10)) is proportional to the quantity Π_{ne} ($\theta \simeq 0.64$), which can have different signs, depending on the parameters entering into this expression. The upper plot in Fig. 10 shows the growth rate as a function of the parameter $p_2 = \omega_{pe}\omega_{be}/(\omega_r^2 - \omega_{ce}^2)$, which depends on the measured values of the plasma density and magnetic field and the semiempirical parameters ω_r and ω_{be}, which can vary within limited ranges. The values of γ^k were obtained for the same beam and plasma parameters as those presented in Fig. 4b. Figure 10 also presents the factors $\Lambda\omega_-$ and Ω_{be}, which largely determine the behavior of γ^k/ω_-. It also follows from Fig. 10 that, along with the beam density and resonance detuning, the main factor governing the development of instability is the beam quality (or its heating). The lower plots Fig. 10 present the measured amplitudes of HF fields and the fluxes of fast protons as functions of the parameter p_2. Since the growth rate can take positive values, $\gamma^k > 0$, for both $\omega \gtrsim \omega_-$ and $\omega \lesssim \omega_-$, the HF measurements were performed at frequencies both higher and lower than the resonant frequency $\omega_-/2\pi \simeq 0.31$–0.35 MHz. The kinetic growth rate was calculated for the former case at $\Delta\omega/2\pi \sim 0.07$–0.09 MHz.

In calculating the growth rates γ^k and γ^h for each particular instant, the resonance detuning $|\Delta\omega|$ was assumed to be constant. Since we first calculated hydrodynamic growth rate (8) (1000×1000 steps over ω and k about their resonant values at every time step), the detuning $\Delta\omega$ was slightly varied about given values in order to satisfy the condition $B^2 - 4AC < 0$ and to choose the optimal parameter values. Taking into account that the beam heating was estimated rather arbitrarily, the absolute value of the detuning can also be chosen arbitrarily within a certain range. The recorded value of the electric field amplitude e_{hf} measured throughout the active experiment at $\omega/2\pi = 0.1$ and 0.5 MHz (see Fig. 10) can be attributed to the cyclotron resonance (similar to the data presented in Fig. 8, which can be attributed to the Cherenkov resonance). Although no explicit correlation between the HF instability and the flux of fast protons was observed, it is not excluded that there may be a mechanism by which the wave energy is transferred from short-scale to long-scale perturbations that are resonant with high-energy proton flows.

Figure 11 presents the results of a comparative analysis of the parameters of HF instability at the first cyclotron harmonic against the excitation of potential waves at $\theta \simeq 0.64$ and $\Delta\omega < 0$ for the initial beam bunching parameters $\Delta\alpha_0 \approx 1.5°$ and $\xi' = 0.85$. The dependence of the instability growth rate and the parameter Π_{1e} on the relative beam heating $p_3 = v_{be}/u$ in the range $p_3^* \simeq 0.07$–0.08 can be divided into two parts. For $v_{be}/u \gtrsim p_3^*$, we have $\Pi_{1e} < 0$; therefore, the growth rate is positive, $\gamma^k > 0$. This is related to the transfer of the electron gyration energy to plasma waves. When $\Pi_{1e} > 0$ ($v_{be}/u \lesssim p_3^*$), the situation is opposite: plasma waves decay due to energy transfer to the beam particles (see Section 3.3). Previously, in considering the instability of a magnetoactive plasma against electromagnetic perturbations in the range of the normal Doppler effect, Zheleznyakov [17] showed that, when electron gyration is taken into account, electromagnetic waves can also be excited at a subluminal electron flow velocity ($u < \omega_\pm/k_z$). Even earlier, the possibility of such an effect for a waveguide excited by an electron flow in a magnetic field was pointed out by Gaponov [18]. Figure 11, which presents the results of measurements of HF electric fields at the frequencies $\omega/2\pi = 0.10$ and 0.25 MHz, compares the observed excitation of cyclotron waves with the calculated BPI parameters. While an increase in the flux of electrons with the energy $\varepsilon_{2e} = 25$ keV is quite predictable, the behavior of the electron flux with $\varepsilon_{2e} = 330$ keV seems to be unexpected. In this paper, we have already considered similar results that were attributed to the scattering of fast electrons in regions with an enhanced level of long-wavelength plasma turbulence. When $\gamma^k/\omega_- < 0$, there may be also an alternative acceleration mechanism related to the absorption of plasma waves by the beam electrons; however, it can hardly provide such a high acceleration rate. Therefore, these results require a more thorough analysis.

The main results of our analysis of the cyclotron excitation of longitudinal HF waves by an electron beam can be formulated as follows:

(i) a comparison of the calculated parameters of instability with the results of active experiments shows that the model of the development of HF cyclotron instability excited by an electron flow in the ionospheric plasma [10, 17] yields satisfactory results, and

(ii) the observed correlation between the excitation of HF waves and the attenuation of the differential fluxes of fast electrons can be attributed to the generation of long-wavelength low-frequency turbulence in the vicinity of the subsatellite.

5. CONCLUSIONS

The excitation of quasi-longitudinal HF waves during BPI and the accompanying effects in the ionospheric plasma have been investigated by using the results from an active experiment on the simultaneous injection of an electron beam with a power of ~1 kW and a xenon ion beam with a power of ~1.2 kW into the ionosphere. The experiment was carried out onboard the *Intercosmos-25* satellite and the *Magion-3* daughter satellite. The injection pitch angles were such that the electron beam propagated through the extended hollow beam of xenon ions having low transverse velocities. The experimental data have been compared with the BPI parameters calculated by using the kinetic and hydrodynamic approaches for different beam–plasma models and different injection modes. The results obtained show that such an analysis is important for studying not only the excitation of electrostatic and electromagnetic waves but also the amplification (generation) of fluctuations of a quasi-steady magnetic field and the acceleration of fast particles. Let us summarize the main results.

Using the theory developed by Kitsenko and Stepanov [10], a satisfactory agreement has been achieved between the calculated parameters of the BPI excited during the injection of a warm electron beam into the cold ionospheric plasma and the HF fields measured at the *Magion-3* subsatellite. Taking into account the finite Larmor radius of the beam electrons (a flow of oscillators) allows one to determine the conditions for the anomalous absorption or excitation of HF waves under the electron-cyclotron resonance conditions. These results are confirmed by the data on the generation of HF waves and 25- to 40-keV electron fluxes recorded by using a DOK-S spectrometer onboard the subsatellite.

In the regime of modulated injection, when the modulation frequency was close to the Langmuir frequency of the beam electrons (calculated for the first harmonic of the convection current), an appreciable decrease in the amplitude of ELF waves and the amplification of lower hybrid and short-period magnetic field fluctuations were observed. Such a resonance can lead to ether the destruction of the beam or its focusing.

When the beam was modulated at a frequency close to the lowest electron plasma frequency (~250 kHz), the subsatellite recorded the amplification of the HF field in the range of the main plasma resonance frequencies. Anomalous induced fields were observed over 2–5 s after the end of electron injection. This is presumably due to the presence of an external beam of heavy xenon ions.

The excitation of HF waves by a warm electron beam is accompanied by the generation of anomalous fluxes of 1-MeV protons. The occurrence of these fluxes is probably related to the generation of Alfvén waves during the propagation of the electron beam inside an ion beam.

ACKNOWLEDGMENTS

We thank all the experts from different international institutions who participated in preparing the APEX project. K. Kudela and J. Matišin acknowledge the support of the Slovak Research and Development Agency, grant no. APVV-51-053805.

REFERENCES

1. V. N. Oraevskiĭ, Ya. P. Sobolev, L. N. Zhuzgov, et al., Fiz. Plazmy **17**, 741 (2001) [Plasma Phys. Rep. **17**, 699 (2001)].
2. N. V. Baranets, Yu. Ya. Ruzhin, V. V. Afonin, et al., Kosm. Nauka Tekhnol. **10** (5), 49 (2000).
3. B. N. Maehlum, K. Maseide, K. Aarsnes, et al., Planet. Space Sci. **28**, 269 (1980).
4. *Artificial Particle Beams in Space Plasma Studies*, Ed. by B. Grandal (Plenum, New York, 1982; Mir, Moscow, 1985).
5. S. I. Kozlov and N. V. Smirnova, Kosm. Issl. **30**, 629 (1992).
6. V. P. Kovalenko, Usp. Fiz. Nauk **139**, 223 (1983) [Sov. Phys. Usp. **26**, 116 (1983)].
7. *Radiophysical Electronics*, Ed. by N. A. Kaptsov (Mir, Moscow, 1978) [in Russian].
8. A. I. Akhiezer, I. A. Akhiezer, R. V. Polovin, et al., *Plasma Electrodynamics* (Nauka, Moscow, 1974; Pergamon, Oxford, 1975).
9. K. N. Stepanov and A. B. Kitsenko, Zh. Tekh. Fiz. **31**, 167 (1961) [Sov. Phys. Tech. Phys. **6**, 120 (1961)].
10. A. B. Kitsenko and K. N. Stepanov, Ukr. Fiz. Zh. **6**, 297 (1961).
11. H. P. Freund, I. Haber, P. Palmadesso, and K. Papadopoulos, Phys. Fluids **23**, 518 (1980).
12. P. M. Banks and W. J. Raitt, J. Geophys. Res. **93**, 5811 (1988).
13. A. S. Volokitin, Yu. Ya. Ruzhin, V. G. Korobeĭnikov, and V. S. Dokukin, Geomagn. Aéron. **40** (3), 133 (2000).
14. N. V. Baranets, Yu. I. Galperin, N. S. Erokhin, et al., Adv. Space Res. **21**, 709 (1998).
15. D. G. Lominadze and K. N. Stepanov, Zh. Tekh. Fiz. **34**, 1823 (1964) [Sov. Phys. Tech. Phys. **9**, 1408 (1965)].
16. J. L. Roeder, W. R. Sheldon, J. R. Benbrook, et al., Ann. Geophys. **36**, 401 (1980).
17. V. V. Zheleznyakov, Izv. Vyssh. Uchebn. Zaved., Radiofiz. **3**, 57 (1960).
18. A. V. Gaponov, Izv. Vyssh. Uchebn. Zaved., Radiofiz. **2**, 443 (1959).

Translated by É.G. Baldina